[15] suggested that the abscopal effect is not tumor-specific but radiation dose dependent. In their animal experiment, they irradiated normal tissue and observed the effects on two types of tumors at a distant site. Their results implicated p53 as a key mediator of the radiation-induced abscopal effect, and suggested that pathways downstream of p53 are important in eliciting this response.

Table 1 summarizes the reports in the literature on abscopal effects observed in clinical studies after RT [2–12]. Clinicians initially attempted to explain the abscopal effect as a radiation-induced increase in the circulating levels of cytokines such as tumor necrosis factor (TNF) [5] or interleukin (IL)-18 [7]. According to a recent clinical report by Postow et al. [12], a patient with NY-ESO-1+ melanoma was treated by local RT and systemic injection of the anti-CTLA antibody ipilimumab, both before and after RT. In this patient, palliative irradiation of a paraspinal thoracic mass led to the regression of distant lesions, in particular a hilar lymphadenopathy of the lung and a splenic lesion. This response was temporarily correlated with signs of an anti-melanoma immune response, namely an increase in NY-ESO-1-specific antibodies, as well as a rise in the frequency of circulating CD4+ T cells expressing the activation marker ICOS, NY-ESO-1-specific interferon gamma-producing CD4+ cells, and HLA-DR-expressing CD14+ monocytes. These data suggest that the abscopal effects of RT are indeed mediated by specific anticancer immune responses.

Recent evidence suggests that local RT can elicit an immune response, and the corresponding effectors (most likely T lymphocytes) then migrate to distant lesions, provoking their regression. RT has the ability to kill cancer cells, and RT-killed cancer cells can be a good source of tumor antigens for inducing cytotoxic T-lymphocyte (CTL) activation. The immune response against other unirradiated malignant cells expressing similar tumor antigens could be augmented. According to an experimental study by Yasuda et al. [16], intratumoral injection of IL-2 not only enhanced shrinkage of the irradiated tumor itself, but also suppressed the development of distant metastasis located outside the RT field, possibly through the induction of a systemic T-cell response. Akutsu et al. [17] reported that a combination of direct intratumoral (i.t.) administration of bone marrow-derived dendritic cells (DCs) and RT in mouse squamous cell carcinoma was able to induce a strong antitumor effect not only against treated local tumors but also against untreated distant tumors. Heat shock protein gp96, also called glucose-regulated protein GRP94, is a stress protein that works as a protein chaperone when DCs take up the antigen via surface molecule CD91 to mediate CTL activation by Toll-like receptors (TLR) 2 and 4. Gp96 is considered a target molecule in explanations of the abscopal effect.

BCG-CWS can activate immature human dendritic cells (iDC), especially bone marrow-derived DC. Although iDC efficiently take up tumor-derived protein/peptides, they barely exhibit antigen presentation or T-cell proliferation. Antigen presentation and T-cell stimulation are enhanced by adjuvants—in this case BCG-CWS, which also induces upregulation of the DC maturation markers CD83 and CD86 and the secretion of inflammatory cytokines such as IL-6, IL-12, and TNF-α. These responses and the increase in antigen-presenting ability, namely cross-presentation, indicate that the activation and maturation of DC is induced by CWS containing mycobacterial peptidoglycan. This suggests that BCG-CWS induces TNF-α secretion from myeloid DC via TLR2 and TLR4, and that the secreted TNF-α induces the maturation of DC [18]. The matured DCs facilitate antigen processing and the loading of tumor-associated antigens into major histocompatibility complex (MHC) class 1 and 2 molecules, which are recognized by CD8 and CD4 T cells, respectively.

Patient 1 remained disease-free at least for 47 months (from August 1999 to June 2003) and then developed left lung adenocarcinoma with brain, lung, and lymph node metastases. No definitive diagnosis as to whether it was a second primary or metastatic lesion was made histologically. However, the new lesion with a tapered bronchus was located in a different place from the lesion that was eliminated through the abscopal effect according to chest CT (Fig. 1).

To date, there has been no description of the time interval between irradiation and the development of the abscopal effect. Postow et al. [12] reported that the abscopal effect was found 4 months after irradiation in a patient with melanoma. In patient 2, two new lesions were detected in the left lung on chest CT about 20 months after SBRT to the right lung metastasis of urothelial carcinoma. Three months after the start of BCG-CWS immunotherapy, the new lesions had completely regressed and this response continued for more than 1 year. How long does immune memory last? Memory T-cell responses were long-lived in the absence of re-exposure to antigens/vaccines/pathogens. Recent studies of anti-smallpox immune memory showed that memory T-cell levels were long-lived but declined with a half-life of 8–15 years [19]. The cross-talk between innate lymphocytes and DC which leads to innate lymphocyte activation and DC maturation is augmented by using a TLR agonist (ligand) such as BCG-CWS. According to a putative mechanism, the booster immunization caused by the administration of BCG-CWS led to a long-term complete response in patient 2.

It is difficult to clearly identify whether the effect was due to BCG-CWS alone, the RT abscopal effect alone, or the RT abscopal effect augmented by BCG-CWS. The targets of pathogen-associated molecular patterns (PAMPs)

**Table 1** Radiation abscopal effects observed in clinical studies

| Reference | Patient | Tumor type | Treatment | Abscopal effects | Duration of regression | Putative modulator of abscopal effects |
|---|---|---|---|---|---|---|
| Lome et al. [2] | 66 years, male | Bladder cancer | RT of primary tumor | 10 M following RT, complete regression of lung metastases | 23 M | |
| Krikorian et al. [3] | 55 years, female | Malignant lymphoma | RT of eyelid tumor | 14 M following RT, complete regression of axillar, abdominal, and parotid adenopathy | 51 M following diagnosis | |
| Rees et al. [4] | 49 years, male | Esophageal adenocarcinoma | RT of the primary esophageal lesion | Regression of lung metastases | 20 M | |
| Ohba et al. [5] | 76 years, male | HCC | RT of thoracic vertebral bone metastases | 10 M following RT, remarkable regression of the primary tumor | 35 M | TNF-α |
| Takaya et al. [6] | 69 years, female | Uterine cervical carcinoma | RT of the primary pelvic lesion | 6 M following RT, complete regression of para-aortic LN metastasis | NR | |
| Nakanishi et al. [7] | 79 years, male | HCC | RT and TAE of the huge HCC with IVC invasion | 5 M following RT, regression of the untreated HCC | NR | Interleukin 18 |
| Formenti et al. [8] | | Thymic carcinoma | RT of primary tumor | Complete regression of lung metastasis | 38 M | GM-CSF |
| Isobe et al. [9] | | Natural killer cell lymphoma | RT of eyelid tumor | Regression of natural killer cell lymphoma | NR | CD8+ T cells |
| Lakshmanagowda et al. [10] | 65 years, female | Chronic lymphocytic leukemia | RT of massive axillary lymphadenopathy | 2 weeks following RT, complete regression of neck lymphadenopathy | 6 M | |
| Okuma et al. [11] | 63 years, male | HCC | RT of the mediastinal LN metastasis | Complete regression of lung metastasis | 10 years | |
| Postow et al. [12] | 39 years, female | Melanoma | RT of the paraspinal metastasis with ipilimumab | Regression of hilar lymphadenopathy and splenic lesion | 11 M | Antibody response to the cancer–testis antigen NY-ESO-1 |
| Our patient 1 | 74 years, male | Adenocarcinoma of the lung | RT of the supraclavicular LN metastasis followed by BCG-CWS | 3 M following RT, complete regression of multiple lung metastasis | 47 M | Dendritic cell CTL |
| Our patient 2 | 62 years, female | Urothelial carcinoma | RT of the right lung metastasis followed by BCG-CWS | 24 M following RT, complete regression of two left lung metastasis | 26 M | Dendritic cell CTL |

*RT* radiation therapy, *M* months, *HCC* hepatocellular carcinoma, *NR* not reported, *TNF* tumor necrosis factor, *TAE* transcatheter arterial embolization, *IVC* inferior vena cava, *GM-CSF* granulocyte macrophage-colony stimulating factor, *LN* lymph node, *CTL* cytotoxic T lymphocyte, *BCG-CWS* cell wall skeleton of *Mycobacterium bovis* bacillus Calmette–Guérin

such as BCG-CWS are not lymphocytes but antigen-presenting cells (APC). Currently, BCG-CWS is potentially most effective in patients with minimal disease such as that after resection, after definitive chemoradiation, or after first-line combination chemotherapy. The clinical response obtained in our patients may not have been achieved through BCG-CWS treatment alone without the coexistence of the immunologic cancer antigens that were released by the tumor necrosis caused by RT. On the other hand, the RT-induced cell death causes the release of endogenous danger signals known as damage-associated molecular patterns (DAMP). These DAMPs augment the presentation of tumor antigens released from necrotic tumor cells, ultimately inducing the immune system to attack cancer, thereby mimicking an acute infection. DAMPs and PAMP (BCG-CWS) may share some commonality of expression [20].

According to our phase II study [14], the IFN-γ level does not always elevate after BCG-CWS induction in patients with advanced cancer and/or prolonged chemotherapy. Namely, if the innate immune system is damaged during the patient's clinical course, innate immunity might not be activated by BCG-CWS induction. Thus, we utilized IFN-γ as a marker of innate immune response but not a surrogate marker of the abscopal effect. IFN-γ induction tests were performed during the relatively early phases of BCG-CWS treatment (at the times of the 4th and 5th inoculations). The level of IFN-γ in the peripheral blood was measured before inoculation and 18 h after the inoculation of BCG-CWS. In patients 1 and 2, an elevation of the serum IFN-γ level was observed after BCG-CWS administration. It is worth noting that patient 1 reacted strongly to BCG-CWS; he presented a skin reaction at the inoculation site as well as the swelling of multiple reactive lymph nodes in the neck and axilla. His serum IFN-γ level was also extremely high. Based on these observations, we suppose that BCG-CWS played a more crucial role than DAMPs in his abscopal effect.

Enhancement of the systemic response after local RT in combination with an effective immune adjuvant such as BCG-CWS may provide new insights and suggest new therapeutic avenues to pursue.

**Acknowledgments** This work was supported in part by a grant from the Osaka Community Foundation. We are grateful to Drs. Kumao Toyoshima, Ichiro Azuma, and Kinji Nishiyama for supporting this work. BCG-CWS was kindly provided by Dr. Ichiro Azuma.

**Conflict of interest** The authors declare that they have no conflict of interest.

## References

1. Mole RH (1953) Whole body irradiation—radiobiology or medicine? Br J Radiol 26:234–241
2. Lome LG, Navani S, Aral IM (1970) Spontaneous regression of pulmonary metastases from transitional cell carcinoma of the bladder. Cancer 26:415–418
3. Krikorian JG, Portlock CS, Cooney DP, Rosenberg SA (1980) Spontaneous regression of non-Hodgkin's lymphoma. A report of nine cases. Cancer 46:2093–2099
4. Rees G, Ross C (1983) Abscopal regression following radiotherapy for adenocarcinoma. Br J Radiol 56:63–66
5. Ohba K, Omagari K, Nakamura T, Ikuno N, Saeki S, Matsuo I, Kinoshita H, Masuda J, Hazama H, Sakamoto I, Kohno S (1998) Abscopal regression of hepatocellular carcinoma after radiotherapy for bone metastasis. Gut 43:575–577
6. Takaya M, Niibe Y, Tsunoda S, Jobo T, Imai M, Kotani A, Unno N, Hayakawa K (2007) Abscopal effect of radiation on toruliform para-aortic lymph node metastases of advanced uterine cervical carcinoma—a case report. Anticancer Res 27:499–504
7. Nakanishi M, Chuma M, Hige S, Asaka M (2008) Abscopal effect on hepatocellular carcinoma. Am J Gastroenterol 103:1320–1321
8. Formenti SC, Demaria S (2009) Systemic effects of local radiotherapy. Lancet Oncol 10:718–726
9. Isobe Y, Aritaka N, Sasaki M, Oshimi K, Sugimoto K (2009) Spontaneous regression of natural killer cell lymphoma. J Clin Pathol 62:647–650
10. Lakshmanagowda PB, Viswanath L, Thimmaiah N, Dasappa L, Supe SS, Kallur P (2009) Abscopal effect in a patient with chronic lymphocytic leukemia during radiation therapy: a case report. Cases J 2:204. doi:10.1186/1757-1626-2-204
11. Okuma K, Yamashita H, Niibe Y, Hayakawa K, Nakagawa K (2011) Abscopal effect of radiation on lung metastases of hepatocellular carcinoma: a case report. J Med Case Rep 5:111. doi:10.1186/1752-1947-5-111
12. Postow MA, Callahan MK, Barker CA, Yamada Y, Yuan J, Kitano S et al (2012) Immunologic correlates of the abscopal effect in a patient with melanoma. N Engl J Med 366:925–931
13. Azuma I, Kishimoto S, Yamamura Y, Petit JF (1971) Adjuvanticity of mycobacterial cell wall. Jpn J Microbiol 15:193–197
14. Kodama K, Higashiyama M, Takami K, Oda K, Okami J, Maeda J et al (2009) Innate immunotherapy with Bacillus Calmette–Guerin (BCG)-cell wall skeleton after radical surgery for non-small cell lung cancer: a case–control study. Surg Today 39:194–200
15. Camphausen K, Moses MA, Mènard C, Sproull M, Beecken WD, Folkman J et al (2003) Radiation abscopal antitumor effect is mediated through p53. Cancer Res 63:1990–1993
16. Yasuda K, Nirei T, Tsuno NH, Nagawa H, Kitayama J (2011) Intratumoral injection of interleukin-2 augments the local and abscopal effects of radiotherapy in murine rectal cancer. Cancer Sci 102:1257–1263
17. Akutsu Y, Matsubara H, Urashima T, Komatsu A, Sakata H, Nishimori T et al (2007) Combination of direct intratumoral administration of dendritic cells and irradiation induces strong systemic antitumor effect mediated by GRP94/gp96 against squamous cell carcinoma in mice. Int J Oncol 31:509–515
18. Tsuji S, Matsumoto M, Takeuchi O, Akira S, Azuma I, Hayashi A et al (2000) Maturation of human dendritic cells by cell wall skeleton of *Mycobacterium bovis* bacillus Calmette–Guerin: involvement of Toll-like receptors. Infect Immun 68:6883–6890
19. Crotty S, Ahmed R (2004) Immunological memory in humans. Semin Immunol 16:197–203
20. Ludgate CM (2012) Optimizing cancer treatment to induce an acute immune response: radiation abscopal effects, PAMPs and DAMPs. Clin Cancer Res 18:4522–4525

# Differentiation of lung neoplasms with lepidic growth and good prognosis from those with poor prognosis using computer-aided 3D volumetric CT analysis and FDG-PET

Daisuke Morimoto, Shodayu Takashima, Naohiro Sakashita, Yoshinobu Sato, Binghu Jiang, Tomoaki Hakucho, Chie Miyake, Yoshiyuki Takahashi, Yasuhiko Tomita, Katsuyuki Nakanishi, Takuya Hosoki and Masahiko Higashiyama

*Acta Radiol* published online 3 September 2013
DOI: 10.1177/0284185113502336

Acta Radiol OnlineFirst, published on September 3, 2013 as doi:10.1177/0284185113502336

*Original Article*

Acta Radiologica
0(0) 1–7

DOI: 10.1177/0284185113502336
acr.sagepub.com



# Differentiation of lung neoplasms with lepidic growth and good prognosis from those with poor prognosis using computer-aided 3D volumetric CT analysis and FDG-PET

**Daisuke Morimoto[1], Shodayu Takashima[1], Naohiro Sakashita[2], Yoshinobu Sato[3], Binghu Jiang[1], Tomoaki Hakucho[1], Chie Miyake[1], Yoshiyuki Takahashi[1], Yasuhiko Tomita[2], Katsuyuki Nakanishi[2], Takuya Hosoki[4] and Masahiko Higashiyama[2]**

## Abstract

**Background:** Many studies have reported that transverse computed tomography (CT) imaging findings correlate with prognosis of patients with small peripheral lung neoplasm with lepidic growth. However, no studies have examined this correlation with the aid of three-dimensional (3D) CT data.

**Purpose:** To determine the most efficacious imaging factor for differentiation of lepidic growth type lung neoplasms with good prognosis from those with poor prognosis.

**Material and Methods:** We evaluated CT findings, nodule patterns, $SUV_{max}$ on FDG-PET/CT, as well as nodule volume and ratios of solid parts to nodule volume that were semi-automatically measured on CT images of 64 pulmonary nodules of $\leq$2 cm in 60 consecutive patients (24 men and 36 women; mean age, 65 years). For logistic modeling, we used all of the significant factors observed between the neoplasms with good and with poor prognosis as independent variables to estimate the statistically significant factors for discriminating invasive adenocarcinomas with lepidic growth (lesions with poor prognosis, $n = 42$) from the other neoplasms, including preinvasive lesions (lesions with good prognosis, $n = 22$), resulting in a recommendation for the optimal criterion for predicting lesions with poor prognosis.

**Results:** The logistic regression model identified the ratio of the solid part to the whole volume of a pulmonary nodule as the only significant factor ($P = 0.04$) for differentiating lepidic growth type lung neoplasms with good prognosis from those with poor prognosis. A ratio of 0.238 or more showed the highest discriminatory accuracy of 84% with 91% sensitivity and 76% specificity.

**Conclusion:** Computer-aided analyses of pulmonary nodules proved most useful for establishing the optimal criterion for differentiation of lepidic growth type lung neoplasms with good prognosis from those with poor prognosis.

### Keywords

Lung cancer, adenocarcinoma, computer-aided diagnosis, PET/CT, $SUV_{max}$

Date received: 27 November 2012; accepted: 30 July 2013

[1]Osaka University Graduate School of Medicine, Division of Allied Health Sciences, Department of Diagnostic Radiological Imaging, Osaka, Japan
[2]Osaka Medical Center for Cancer and Cardiovascular Diseases, Osaka, Japan
[3]Osaka University Graduate School of Medicine, Department of Radiology, Osaka, Japan
[4]Morinomiya Clinic, Osaka, Japan

**Corresponding author:**
Daisuke Morimoto, Osaka University Graduate School of Medicine, Division of Allied Health Sciences, Department of Diagnostic Radiological Imaging, 1-7 Yamadaoka, Suita, Osaka 565-0871, Japan.
Email: m.daisuke@cure.ocn.ne.jp

## Introduction

Lung cancer is the most common and the leading cause of cancer death in developing countries (1), with a dramatic shift recently having occurred in the incidence rates of histologic subtypes of lung cancer (2). After a steady increase in incidence since 1973, adenocarcinoma replaced squamous cell carcinoma in many countries as the most frequent histologic subtype of lung cancer. This overall increase in adenocarcinoma is largely due to a marked increase in adenocarcinomas with pure lepidic growth (3).

Noguchi et al. (4) classified small adenocarcinoma of the lung (≤2 cm) into six subtypes and investigated their correlation with prognosis. Subtypes types A, B, and C featured components of lepidic tumor growth, and the remaining types showed destructive tumor growth only. The researchers reported that patients with types A and B, which correspond to solitary adenocarcinomas with pure lepidic growth according to the most recent classification, had good prognosis with a 5-year survival rate of 100%, while patients with type C, which corresponds to invasive adenocarcinoma with lepidic growth, showed poorer prognosis with a 5-year survival rate of 75% (4,5).

Thin-section computed tomography (TSCT) can indicate underlying pathologic conditions of lung cancer. On TSCT, the lepidic growth appears as a ground-glass opacity (GGO) area, while the destructive tumor appears as a solid mass (6,7). Therefore, type A tumor shows a GGO pattern, type B a GGO or mixed GGO pattern, while type C shows a mixed GGO or a solid pattern. Thus, it is of clinical importance to use TSCT for discriminating type A and B tumors from type C because this differentiation aids prognostic prediction and selection of an appropriate surgical method for patients with this type of neoplasm.

Several studies have used ratios of GGO areas to pulmonary nodules obtained from transverse TSCT imaging or 18F-fluorodeoxy glucose positron emission tomography (FDG-PET) findings for predicting prognosis of patients with small adenocarcinoma of the lung (8,9). To our knowledge, however, no studies have been reported in which three-dimensional (3D) analyses of pulmonary nodules using TSCT data were used for this purpose. In the current study, we investigated if the ratio of GGO to the whole pulmonary nodule measured semi-automatically on TSCT images and determined with computer-aided calculations is useful for prognostic prediction among small adenocarcinoma with lepidic growth in the lung.

## Material and Methods

### *Patients and histology of pulmonary nodules*

This retrospective study received institutional review board approval and included 60 consecutive patients (24 men and 36 women; mean age, 64.9 years; age range, 31–81 years) who underwent surgical resection of solitary pulmonary nodules between June 2006 and December 2008 at a medical center. All patients were examined with TSCT scans and FDG-PET/CT prior to surgery. The mean interval between CT and PET/CT studies and surgery was 17 (range, 1–30 days) and 16 days (range, 2–28 days), respectively. None of the patients had serum blood sugar levels exceeding 200 mg/dl at the time of PET/CT examinations. Resected nodules were classified into two subtypes according to prognosis: good prognosis, including atypical adenomatous hyperplasias (AAH) and adenocarcinomas with pure lepidic growth, and poor prognosis, including invasive adenocarcinoma with lepidic growth.

### *Imaging techniques*

All CT images were acquired with a 16 detector-row CT machine (Aquilion 16; Toshiba, Tokyo, Japan) using the following CT parameters: 120 kV X-ray tube voltage, 150-250mA tube current, 35 cm field of view (FOV), 16 × 0.5 mm collimations, a 1.5 helical pitch. All CT images were reconstructed with the aid of a lung reconstruction kernel.

FDG-PET-CT scan was performed with the use of two scanners, Biograph Duo (Siemens, Erlangen, Germany) with two lines of detectors, and Gemini (Philips Medical Systems, Best, The Netherlands) with 16 lines of detectors. All patients fasted and rested for at least 6 h and subsequently received 3.7 MBq/kg of FDG intravenously followed by PET-CT scanning after another hour of rest. PET and CT scans were obtained from vertex to femur during free breathing. Averaged acquisition time was 20 min per patient.

### *Evaluation of TSCT findings*

Two experienced chest radiologists (ST and KN) independently investigated all CT images while blinded to clinical data and determined the presence or absence of lobulation, coarse spiculation, pleural tag, and air bronchogram of the pulmonary nodules based on consensus. The consensus method was used to resolve discordant results. All CT images were reviewed with a fixed lung window (level = −600 HU; width = 1200 HU). The same radiologists also investigated nodular patterns on CT

images and classified them into three patterns (solid, mixed GGO, and GGO).

*Maximum standardized uptake values ($SUV_{max}$).* For the FDG-PET/CT studies, two experienced PET radiologists (TH and ST) independently measured the maximum standard uptake value ($SUV_{max}$) for each lesion. The $SUV_{max}$ were obtained by selecting volumetric regions of interest within each pulmonary nodule to include all tumor tissue but not any non-tumor tissue with potentially higher $SUV_{max}$ than that of the tumor. $SUV_{max}$ was calculated with the following formula (10):

$$SUV = \frac{\text{Counts.CF[kBq/ml/kg]}}{\text{ID[KBq/ml]/mass[kg]}} \times \text{Decay factor}$$

where CF stands for calibration factor and ID for injected dose. Attenuation-corrected PET images were used for the calculations, and averaged values of $SUV_{max}$ determined by the two radiologists were used for analyses.

### 3D volumetric measurement

A researcher (NS) together with a chest radiologist (ST) and another researcher (DM) together with a different thoracic radiologist (KN) used the 3D volumetric CT data to independently measure the entire volume and the solid part of each pulmonary nodule. For these measurements, first a region of interest (ROI) comprising the entire pulmonary nodule was placed on the CT images (Fig. 1a). Next, the nodule was segmented from the surrounding normal lung by using visually determined optimal thresholds of the CT values (Fig. 1b), which had been determined beforehand with the Otsu method (11) and finally the adjacent pleura and vessels were manually excluded.

We then measured the volume of the solid part of each mixed GGO nodule by creating CT value histograms for the extracted entire nodules. From these we obtained the optimal threshold for delineating the solid part from the GGO areas by means of the Otsu method and calculated the volume of the solid part by counting the number of voxels of corresponding areas (Fig. 1c). Next, we calculated the ratios (expressed ratio) of the volume of the solid part to the volume of the nodule for each nodule (Fig. 1d). The averaged values of the two measurements were used for analyses.

*Statistical analyses.* We examined statistically significant differences in all of the CT findings, PET $SUV_{max}$, and 3D volumetric CT analyses between neoplasms with good and with poor prognosis. Fisher's exact test or chi-square tests were used for the assessment of CT findings and Student's t-test for the assessment of $SUV_{max}$ and 3D volumetric CT analyses results. For logistic regression modeling, we used the statistically significant factors as independent variables for differentiating the two groups. Finally, we assessed the diagnostic statistics for predicting which tumors had poor prognosis and recommendation of the optimal criterion. A $P$ value $<0.05$ was considered to indicate a statistically significant difference. All of the statistical calculations were performed using SPSS software (SPSS Inc., Chicago, IL, USA).

## Results

A total of 64 pulmonary nodules measuring 2 cm or less were resected by surgery, 22 of which were of the good prognosis subtype (3 atypical adenomatous hyperplasias [AAH] and 19 adenocarcinomas with pure lepidic growth) and 42 of the poor prognosis subtype (42 invasive adenocarcinomas with lepidic growth). As shown in Table 1, a statistically significant difference between these two groups was seen in the prevalence of pleural tags ($P=0.01$) and nodular patterns ($P<0.001$) as well as in the mean values of PET $SUV_{max}$ ($P=0.001$), nodule volume ($P=0.02$), solid part volume ($P<0.001$), and the ratios of solid part to total nodule volume ($P<0.001$). The average time for volume measurement was 5 min per nodule.

Logistic regression analyses revealed that the ratio of solid part to nodule volume was the only significant independent variable for differentiating the two tumor groups ($P=0.04$). Table 2 shows the relationships between the thresholds for ratios of solid part to nodule volume and diagnostic statistics for prediction of tumors with poor prognosis. A ratio of 0.238 or greater yielded the highest predictive accuracy of 84%, but this included six false-positive and four false-negative diagnoses. A threshold of 0.592, on the other hand, yielded the highest specificity of 96% with 52% sensitivity, 67% accuracy, and 96% positive predictive value. A threshold of 0.046 yielded 100% sensitivity with 36% specificity, 78% accuracy, and 100% negative predictive value.

## Discussion

There are two main types of volume measurement methods of pulmonary nodules: semi-automatic and manual (12–14). For semi-automatic measurement, various algorithms are employed to isolate the nodules from adjacent structures such as surrounding lung parenchyma, vessels, or pleural surface (13,14). Whichever

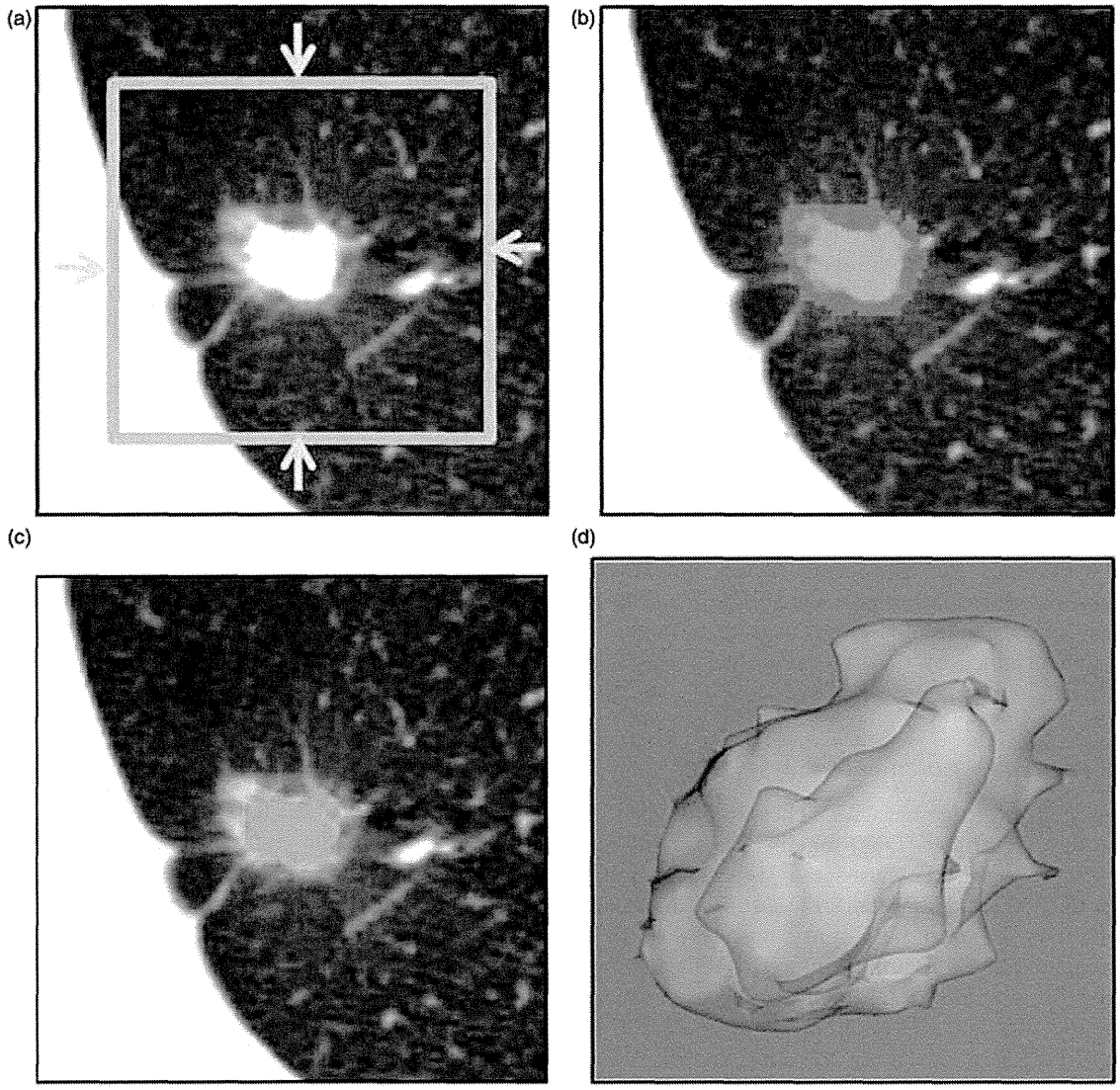


**Fig. 1.** 3D volumetric measurement of a mixed GGO nodule in a 54-year-old man. (a) A region of interest (arrows) was placed on CT images which encompassed the entire pulmonary nodule. (b) The nodule was then segmented from the surrounding normal lung by using visually determined optimal thresholds for CT values, followed by manual exclusion of the adjacent pleura and vessels. (c) CT histograms were created for the entire nodule volume area, yielding data with which we obtained the optimal threshold for separation of the solid part from the GGO areas with the aid of the Otsu method and subsequent extraction of the solid part of the nodule. (d) Surface rendering images of the entire nodule and of the solid part. The entire nodule is shown in white and the solid part in yellow.

method is chosen, however, the final goal is that the values for the segmented nodule approximate as much as possible those for the nodule as characterized by experienced chest radiologists. Nodule volume measurement is widely used for assessment of response to therapy and for calculating volume doubling time with the aid of two serial CT scans to predict malignancy (15–18).

In our study, pulmonary nodules were delineated from surrounding tissues with the Otsu method and manual tracing based on the directions of experienced chest radiologists. For separating the GGO from the solid part in mixed GGO nodules, the optimal threshold of CT values using CT histograms comprising both the GGO and the solid part as well as manual segmentation was used. Although our segmentation methods were traditional, our findings should be clinically relevant, because visual assessment of chest radiologists was used as the gold standard. In addition, we separately delineated the GGO and solid part in mixed GGO

**Table 1.** Comparison of results of thin-section CT and PET/CT findings, and 3D volume measurement of pulmonary nodules with good prognosis and poor prognosis.

| Factors | Good prognosis ($n=22$) | Poor prognosis ($n=42$) | $P$ |
|---|---|---|---|
| Lobulation (%) | 45 (10 of 22) | 69 (29 of 42) | 0.11 |
| Coarse spiculation (%) | 9 (2 of 22) | 26 (11 of 42) | 0.19 |
| Pleural tag (%) | 32 (7 of 22) | 67 (28 of 42) | 0.01 |
| Air bronchogram (%) | 50 (11 of 22) | 74 (31 of 42) | 0.10 |
| Nodule pattern (%) | | | <0.01 |
| Solid | 4 (1 of 22) | 38 (16 of 42) | <0.01 |
| Mixed GGO | 64 (14 of 22) | 62 (26 of 42) | 0.89 |
| GGO | 32 (7 of 22) | 0 | <0.01 |
| PET- $SUV_{max}$* | 0.75 ± 0.46 | 2.41 ± 1.99 | <0.01 |
| Nodule volume ($mm^3$)* | 1161 ± 1179 | 1949 ± 1241 | 0.02 |
| Volume of solid part ($mm^3$)* | 267 ± 393 | 1169 ± 903 | <0.01 |
| Ratio of solid part to nodule volume (%)* | 19.3 ± 23.8 | 64.3 ± 31.9 | <0.01 |

*Data are expressed as mean value ± standard deviation.
Nodules with good prognosis include atypical adenomatous hyperplasia and adenocarcinoma in situ and those with poor prognosis include invasive adenocarcinoma with lepidic tumor growth.

**Table 2.** Relationships between ratios of volume of solid part to that of entire nodule and diagnostic statistics for prediction of tumors with poor prognosis.

| | | | | Predictive value (%) | |
|---|---|---|---|---|---|
| Cut-off values (%) | Sensitivity (%) | Specificity (%) | Accuracy (%) | Positive | Negative |
| ≥4.6 | 100 (42 of 42) | 36 (8 of 22) | 78 (50 of 64) | 75 (42 of 56) | 100 (8 of 8) |
| ≥14.1 | 98 (41 of 42) | 50 (11 of 22) | 81 (61 of 64) | 79 (41 of 52) | 92 (11 of 12) |
| ≥23.8 | 91 (38 of 42) | 73 (16 of 22) | 84 (54 of 64) | 86 (38 of 44) | 80 (16 of 20) |
| ≥59.2 | 52 (22 of 42) | 96 (21 of 22) | 67 (43 of 64) | 96 (22 of 23) | 51 (21 of 41) |
| ≥61.8 | 50 (21 of 42) | 96 (21 of 22) | 67 (43 of 64) | 96 (21 of 22) | 50 (21 of 42) |

nodules and used the result for prediction of small invasive adenocarcinoma with lepidic tumor growth. To our knowledge, such a trial has not been reported in the literature.

Several studies in which tumor grading of small adenocarcinoma was found to correlate with radiologic findings obtained with TSCT or FDG-PET have been published (8,9). Takashima et al. (8) evaluated various thin-section CT findings to differentiate invasive adenocarcinoma with lepidic growth from adenocarcinoma in situ and suggested that percentage of GGO areas of the lesion on transverse TSCT images were most useful for this purpose. Maeda et al. (9) reported that the use of PET $SUV_{max}$ resulted in discrimination between the two categories with 93% accuracy. Takashima et al. (8) further found that the prevalence of coarse spiculation in invasive adenocarcinoma with lepidic growth was statistically significantly greater than that in adenocarcinomas in situ. Moreover, Aoki et al. (19) mentioned in a study of lung adenocarcinomas <3 cm that the presence of coarse spiculation was a significant prognostic factor for predicting poor prognosis. In our study, however, no significant difference was seen in the prevalence of coarse spiculation between neoplasms with good and poor prognosis. This discrepancy may be due to the small number of patients and biased patient population in our study.

Our multivariate analyses indicated that the ratio of the volume of the solid part to that of the entire pulmonary nodule was the only significant factor for differentiating tumors with good prognosis from those with poor prognosis. Our study further suggested that this ratio was more effective than the actual volume of the solid part or the actual nodule volume. The optimal diameter (in pathologic specimens) and area of the solid part (measured on transverse CT images) that represents invasive components of tumors have been proposed as useful for prediction of prognosis for small adenocarcinomas (6,7). However, we believe such measurements are likely to vary widely since they

depend on the pathologic specimens or CT images used so that inter-observer or inter-institutional variability will be high compared to the exact 3D volume measurement employed for the current series. However, we must bear in mind that the capability of PET-CT may have been underestimated in our study because of the inaccuracy of $SUV_{max}$ caused by the partial volume effect in small nodules and by the fact that no special attempt was made or device used to reduce respiratory motion in our PET-CT studies (20,21).

In recent years, many investigators have suggested that limited surgery such as a wide wedge resection, segmentectomy, or lobectomy with hilar lymph node dissection and mediastinal node sampling is advisable for patients with adenocarcinoma in situ (22,23). Yamamoto et al. (23) documented that 5-year survival of patients with early-stage lung cancer, who underwent limited surgery with video assistance, was comparable to that of patients who underwent standard thoracotomies. However, preoperative selection of candidates for limited surgery is a major clinical challenge. In our study, a ratio of 0.238 for the volume of the solid part to that of the entire pulmonary nodule yielded the highest accuracy of 84% for differentiating invasive adenocarcinoma with lepidic growth from adenocarcinoma in situ. A ratio of >0.046 identified adenocarcinoma in situ with 100% sensitivity and a ratio of >0.59 showed the highest positive predictive values of 96% for tumors with poor prognosis. This leads us to believe that 3D volumetric analyses of pulmonary nodules combined with TSCT can be helpful for the selection of appropriate surgical procedures and may enhance the confidence of surgeons for selecting appropriate surgical methods. We suggest that patients with a pulmonary neoplasm with a ratio of <0.046 may be candidates for limited surgery, while patients with a pulmonary neoplasm with a ratio of >0.59 should undergo standard thoracotomy.

According to recent reports, adenocarcinomas with lepidic growth include a category of minimally invasive adenocarcinoma, which contains small invasive components only and therefore has an excellent prognosis with 100% 5-year survival, which is similar to that of adenocarcinoma in situ (5,24,25). Discrimination between small adenocarcinomas with good prognosis, comprising adenocarcinoma in situ as well as minimally invasive adenocarcinoma, and lepidic predominant adenocarcinomas with poor prognosis can be expected to become an important clinical issue and therefore the subject of future studies. Such studies should be performed with the aim to attain accurate prognosis for such aspects as 5-year survival or tumor recurrence.

There are several limitations to our study. First, we used semi-automatic, computer-aided methods to delineate pulmonary nodules from surrounding tissues and to distinguish between the GGO and the solid part in a mixed GGO nodule. The entire procedure took about 5 min per pulmonary nodule. Since delineation of the GGO from the solid part in a mixed GGO nodule is clinically useful as verified in our series, more sophisticated and accurate methods using automatic calculation of ratios of the volume of solid components to that of an entire mixed GGO nodule should be developed. Second, the number of patients was small and our study was retrospective. Third, we could only differentiate between lepidic type lung neoplasms with poor prognosis and those with good prognosis but not perform survival analysis because of the limited number of patients and follow-up periods. We therefore suggest that a future prospective study with a large number of patients should be carried out, which includes analysis of correlation with survival.

## Acknowledgements

We thank Takahashi Horinouchi for his help in collecting CT data.

## Funding

This research received no specific grant from any funding agency in the public, commercial, or not-for-profit sectors.

## References

1. Ferlay J, Shin HR, Bray F, et al. Estimates of worldwide burden of cancer in 2008: GLOBOCAN 2008. Int J Cancer 2010;127:2893–2917.
2. Barsky SH, Cameron R, Osann KE, et al. Rising incidence of bronchioloalveolar lung carcinoma and its unique clinicopathologic features. Cancer 1994;73:1163–1170.
3. Auerbach O, Garfinkel L. The changing pattern of lung carcinoma. Cancer 1991;68:1973–1977.
4. Noguchi M, Morikawa A, Kawasaki M, et al. Small adenocarcinoma of the lung. Histologic characteristics and prognosis. Cancer 1995;75:2844–2852.
5. Travis WD, Brambilla E, Noguchi M, et al. International association for the study of lung cancer/American thoracic society/European respiratory society international multidisciplinary classification of lung adenocarcinoma. J Thorac Oncol 2011;6:244–285.
6. Takashima S, Maruyama Y, Hasegawa M, et al. CT findings and progression of small peripheral lung neoplasms having a replacement growth pattern. Am J Roentgenol 2003;180:817–826.
7. Vazquez M, Carter D, Brambilla E, et al. Solitary and multiple resected adenocarcinomas after CT screening for lung cancer: histopathologic features and their prognostic implications. Lung Cancer 2009;64:148–154.
8. Takashima S, Li F, Maruyama Y, et al. Discrimination of subtypes of small adenocarcinoma in the lung with thin-section CT. Lung Cancer 2002;36:175–182.

9. Maeda R, Isowa N, Onuma H, et al. The maximum standardized uptake values on positron emission tomography to predict the Noguchi classification and invasiveness in clinical stage IA adenocarcinoma measuring 2 cm or less in size. Interact Cardiovasc Thorac Surg 2009;9:70–73.
10. Agarwal M, Brahmanday G, Bajaj SK, et al. Revisiting the prognostic value of preoperative (18)F-fluoro-2-deoxyglucose ((18)F-FDG) positron emission tomography (PET) in early-stage (I & II) non-small cell lung cancers (NSCLC). Eur J Nucl Med Mol Imaging 2010; 37:691–698.
11. Otsu N. A threshold selection method from gray-level histograms. IEEE Trans Syst Man Cybern 1979;9:62–66.
12. Gavrielides MA, Kinnard LM, Myers KJ, et al. Noncalcified lung nodules: volumetric assessment with thoracic CT. Radiology 2009;251:26–37.
13. Kostis WJ, Reeves AP, Yankelevitz DF, et al. Three-dimensional segmentation and growth-rate estimation of small pulmonary nodules in helical CT images. IEEE Trans Med Imaging 2003;22:1259–1274.
14. Diciotti S, Picozzi G, Falchini M, et al. 3-D segmentation algorithm of small lung nodules in spiral CT images. IEEE Trans Inf Technol B 2008;12:7–19.
15. Park CM, Goo JM, Lee HJ, et al. Persistent pure ground-glass nodules in the lung: interscan variability of semiautomated volume and attenuation measurements. Am J Roentgenol 2010;195:W408–W414.
16. Oda S, Awai K, Murao K, et al. Computer-aided volumetry of pulmonary nodules exhibiting ground-glass opacity at MDCT. Am J Roentgenol 2010;194:398–406.
17. Rampinelli C, De Fiori E, Raimondi S, et al. In vivo repeatability of automated volume calculations of small pulmonary nodules with CT. Am J Roentgenol 2009;192:1657–1661.
18. Goodman LR, Gulsun M, Washington L, et al. Inherent variability of CT lung nodule measurements in vivo using semiautomated volumetric measurements. Am J Roentgenol 2006;186:989–994.
19. Aoki T, Tomoda Y, Watanabe H, et al. Peripheral lung adenocarcinoma: correlation of thin-section CT findings with histologic prognostic factors and survival. Radiology 2001;220:803–809.
20. Werner MK, Parker JA, Kolodny GM, et al. Respiratory gating enhances imaging of pulmonary nodules and measurement of tracer uptake in FDG PET/CT. Am J Roentgenol 2009;193:1640–1675.
21. Soret M, Bacharach SL, Buvat I. Partial-volume effect in PET tumor imaging. J Nucl Med 2007;48:932–945.
22. Roviaro G, Varoli F, Vergani C, et al. Long-term survival after videothoracoscopic lobectomy for stage I lung cancer. Chest 2004;126:725–732.
23. Yamamoto K, Ohsumi A, Kojima F, et al. Long-term survival after video-assisted thoracic surgery lobectomy for primary lung cancer. Ann Thorac Surg 2010; 89:353–359.
24. Borczuk AC, Qian F, Kazeros A, et al. Invasive size is an independent predictor of survival in pulmonary adenocarcinoma. Am J Surg Pathol 2009;33:462–469.
25. Yim J, Zhu LC, Chiriboga L, et al. Histologic features are important prognostic indicators in early stages lung adenocarcinomas. Mod Pathol 2007;20:233–241.

# *Pleural recurrence after surgery for pleomorphic adenoma arising from peripheral lung: computed tomography-guided percutaneous needle biopsy as a possible mechanism of local failure*

**Toshiteru Tokunaga, Hidenori Kunou, Daisuke Ishida, Takashi Kanou, Jiro Okami, Yasuhiko Tomita & Masahiko Higashiyama**

**General Thoracic and Cardiovascular Surgery**

ISSN 1863-6705

Gen Thorac Cardiovasc Surg
DOI 10.1007/s11748-013-0310-9

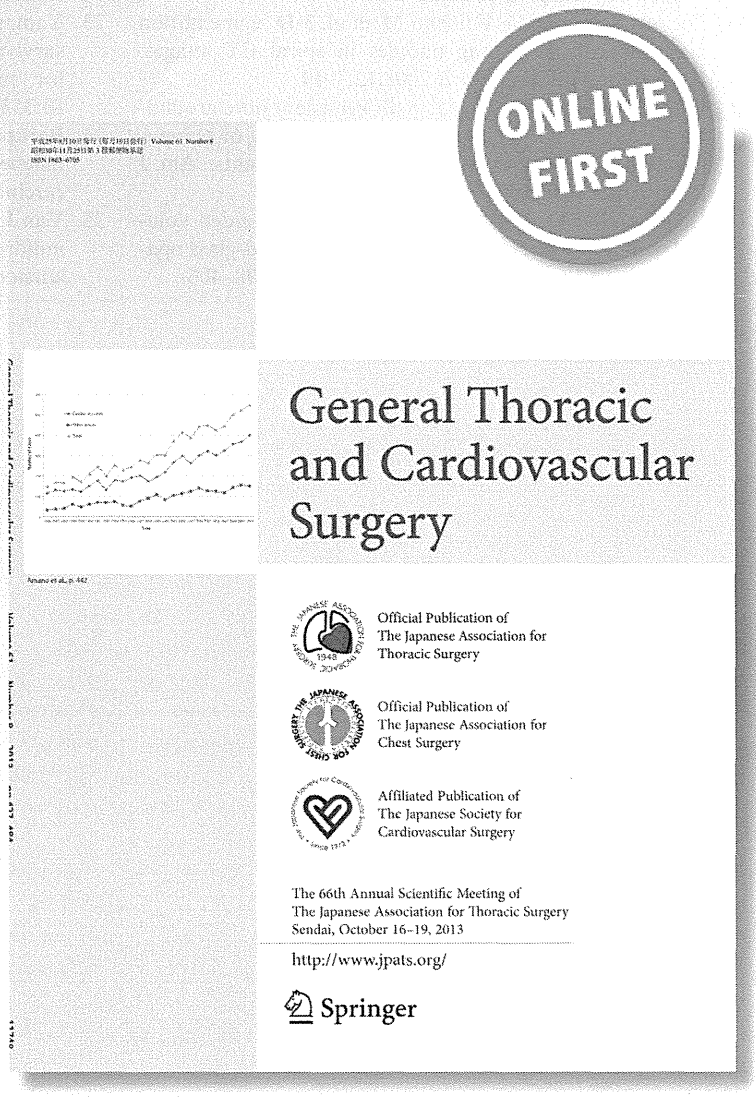


Springer

Gen Thorac Cardiovasc Surg
DOI 10.1007/s11748-013-0310-9

CASE REPORT

# Pleural recurrence after surgery for pleomorphic adenoma arising from peripheral lung: computed tomography-guided percutaneous needle biopsy as a possible mechanism of local failure

**Toshiteru Tokunaga · Hidenori Kunou · Daisuke Ishida · Takashi Kanou · Jiro Okami · Yasuhiko Tomita · Masahiko Higashiyama**

Received: 17 April 2013 / Accepted: 9 August 2013


**Abstract** A 75-year-old male was referred to our hospital because of an abnormal shadow found in the right lung 2 years prior that had been increasing in size. Chest computed tomography showed a 1-cm well-defined nodule in the periphery of the right middle lobe. Although a computed tomography-guided percutaneous needle biopsy was performed, the results were indeterminate. In observations over the course of 1 year, the tumor size increased. Surgical resection was finally performed for diagnosis and treatment, and histological findings revealed a pulmonary pleomorphic adenoma. 2 years after surgery, pleural dissemination unfortunately developed. We present here a case of recurrence as pleural dissemination despite complete resection of a pulmonary pleomorphic adenoma arising from peripheral lung tissue. There is a possibility that the local failure is related to percutaneous needle biopsy.

**Keywords** Pulmonary pleomorphic adenoma · Peripheral lung · Malignant potential

T. Tokunaga (✉) · H. Kunou · D. Ishida · T. Kanou · J. Okami · M. Higashiyama
Department of Thoracic Surgery, Osaka Medical Center for Cancer and Cardiovascular Diseases, 1-3-3 Nakamichi, Higashinari-ku, Osaka 537-8511, Japan
e-mail: tokunaga-to@mc.pref.osaka.jp

Y. Tomita
Department of Pathology, Osaka Medical Center for Cancer and Cardiovascular Diseases, Osaka, Japan

## Introduction

A pleomorphic adenoma is a mixed tumor most commonly presented in the salivary gland, while it rarely occurs in the lung, where it is typically presented as an endobronchial polypoid mass in the proximal airway [1]. This tumor is generally regarded as benign in histopathology findings, though malignancy and aggressive behavior, such as local recurrence, have been reported [2–6]. Herein, we report a case of pleomorphic adenoma arising from peripheral lung tissue in which recurrence was presented as pleural dissemination after surgery, and discuss its possible mechanism of local failure.

## Case

A 75-year-old male was referred to our hospital because of an abnormal shadow in the right lung field, which was incidentally noticed on chest computed tomography (CT) images obtained 2 years prior and then observed as an inflammatory lesion, with a gradual increase in size during follow-up examinations. The patient had undergone a wedge resection of the right upper lobe due to tuberculosis about 50 years previous to his visit to our institution, though there was no past history or present illness related to the salivary glands. A physical examination showed no abnormal findings and laboratory results including serum tumor markers were within normal limits. Chest X-ray imaging showed a nodular shadow in the right middle lung field and a chest CT examination revealed a 1-cm well-defined nodule located in the periphery of the right middle lobe (Fig. 1). Positron emission tomography (PET) showed accumulation of 18F-fluorodeoxyglucose (FDG) with a maximum standardized uptake value (SUVmax) of 1.6.

Published online: 21 August 2013

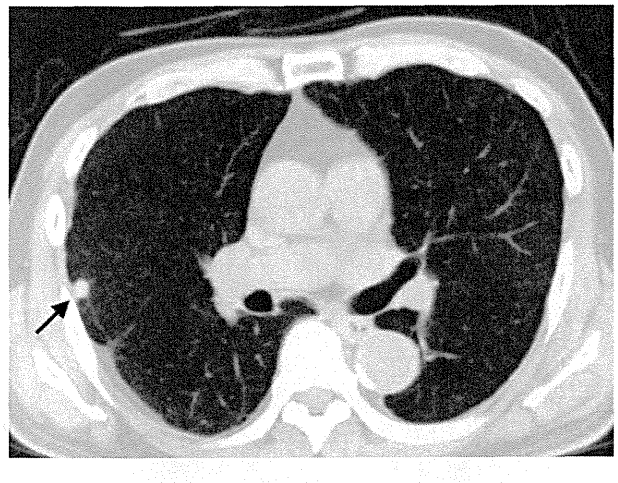

**Fig. 1** Chest computed tomography image showing a 1-cm well-defined nodule in the right middle lobe

**Fig. 2** Gross findings of the tumor showing a well-circumscribed solid mass

A CT-guided percutaneous needle biopsy (CTGNB) of the pulmonary nodule revealed fibrous connective tissue without malignant cells. We continued to follow the patient and noted that the tumor size had enlarged to 1.3 cm after 1 year, thus surgical resection was planned. A wide wedge resection of the right middle lobe was performed through a right lateral muscle-sparing thoracotomy, because he was compromised with chronic obstructive pulmonary disease. The tumor was found adhered to the parietal pleura, while pleural lavage cytology did not reveal any malignant cells. Macroscopic findings showed it to be a well-circumscribed solid mass, 1.3 cm in size (Fig. 2). The distance from the surgical margin to the tumor was more than 2 cm, and the margin cytology was negative. The histological findings revealed a ductal structure with 2 layers and myxoid stromal components (Fig. 3a). The ductal components were composed of cells with scant nuclear atypia in the inner layer and cells with clear cytoplasm in the outer layer (Fig. 3b). Immunohistochemical staining resulted in the former that showed positive for cytokeratin AE1/AE3 (Fig. 3c), while the latter was positive for α-smooth muscle actin (Fig. 3d). Based on histological findings, the tumor was diagnosed as a primary pulmonary pleomorphic adenoma. Although it was morphologically benign, we made a diagnosis of low grade malignancy, because visceral pleural surface invasion was histologically suspected.

2 years after the operation, the patient complained of dyspnea and consulted another hospital, where a chest X-ray showed right pleural effusion. Thoracentesis was performed, after which pneumothorax was incidentally noted and he was subsequently admitted to our hospital. Chest CT findings revealed several pleural masses (Fig. 4). An intercostal chest drain was inserted and bloody fluid was drained, though pneumothorax was not improved and an air leak persisted. On day 8 after drainage, surgical repair of the air leak was performed, while incisional biopsy of only the pleural lesion was performed, as it had extensively invaded the chest wall. A histological examination of the biopsy specimen was similar to the primary lesion (Fig. 5). Thus, it was diagnosed as pleural recurrence of pulmonary pleomorphic adenoma. Thereafter, the patient refused more treatment, but was doing well at 1 year after the latest operation.

## Discussion

Pleomorphic adenomas are most commonly found in salivary glands and rarely encountered in the lungs. Typically, these tumors arise from the bronchial glands and are presented as endoluminal polypoid lesions in the bronchial tree [1]. In contrast, the present case was diagnosed as a primary pleomorphic adenoma located in a peripheral portion of the lung, because no primary lesion was seen with PET imaging. To the best of our knowledge, only 10 cases of pleomorphic adenoma arising from the periphery of the lung have been published in English [5–10]. The clinical characteristics of these cases including ours are presented in Table 1. The patients (8 women, 2 men) ranged from 22 to 76 years old, with an average of 51 years. Eight were asymptomatic, while 2 had symptoms attributable to the tumors. The tumor sizes ranged in size from 1.3 to 4.5 cm. Nine patients had no metastasis and underwent surgical treatment. In the other patient (Case 6), bone, lymph node, liver, and lung metastases were found, and palliative radiation therapy was performed for lumbago due to bone metastasis. Recurrence was seen in only 2 patients, including the present case.

A pleomorphic adenoma is histologically accepted as a benign neoplasm characterized by a biphasic histologic appearance, and consists of epithelial/myoepithelial and

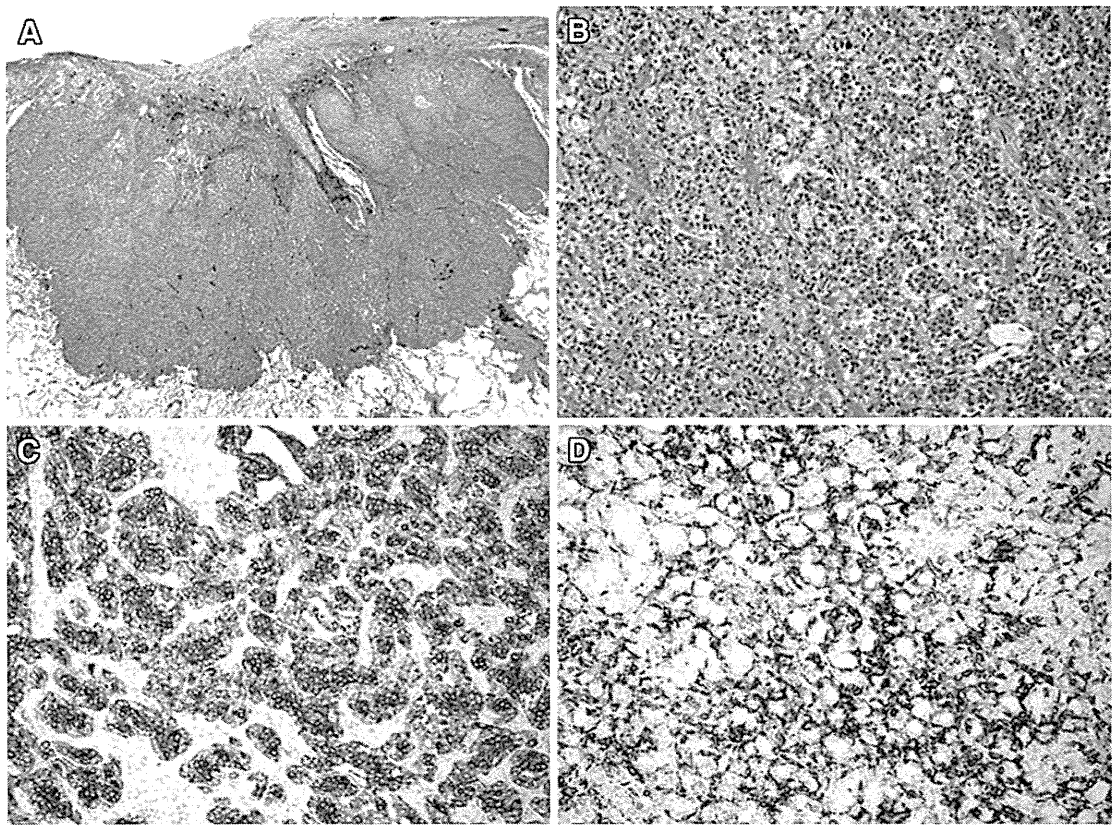


**Fig. 3** **a** Microscopic findings of the tumor showed a biphasic morphology, with ductal structures and myxoid stromal components (H&E ×10). **b** The ductal components consisted of epithelium with scant nuclear atypia and myoepithelium with clear cytoplasm (×50). Immunohistochemical staining was positive for **c** cytokeratin AE1/AE3 (×50) and **d** α-smooth muscle actin (×50)

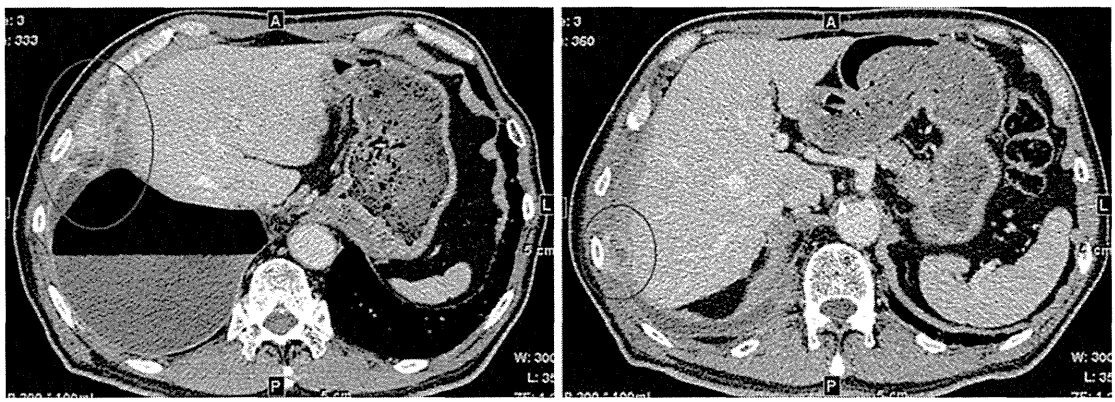

**Fig. 4** Chest computed tomography image showing pleural masses

stromal components [11]. The main treatment is a surgical resection, though this tumor occasionally recurs locally or demonstrates metastasis [11, 12]. Moran et al. [1] reported that a high mitotic count, necrosis, and prominent cellular atypia were associated with aggressive behavior. Among previously reported cases of pulmonary pleomorphic adenoma, 6 developed recurrence or metastasis after the initial operation [2–5]. The clinical characteristics of those patients are shown in Table 2. Those cases consisted of 3 men and 3 women, and their ages ranged from 35 to 76 years old, with a mean of 58.7 years. The resected tumors ranged in size from 1.3 to 16 cm and tumor recurrence occurred within 2–9 years. Lesions that were larger, more infiltrative, or poorly circumscribed tended to recur earlier after the operation. Therefore, this neoplasm should be treated clinically as malignancy.

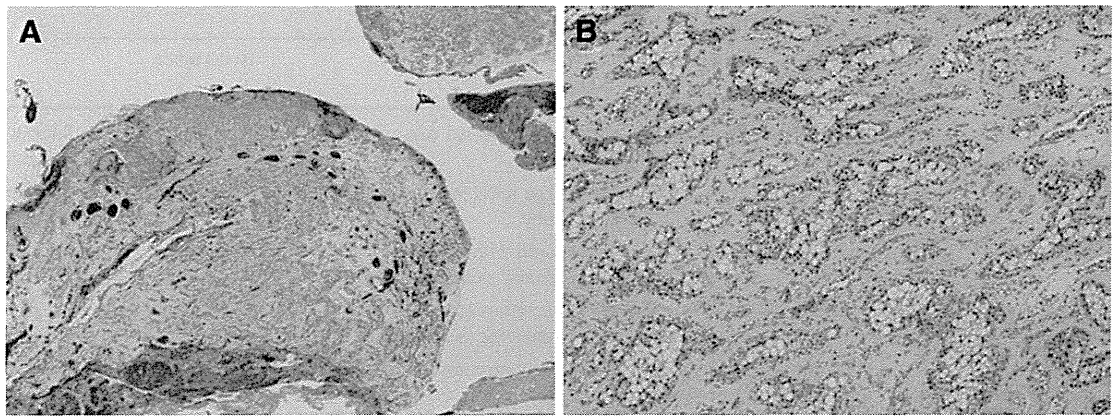


**Fig. 5** Histological examination showed proliferation of tumor cells arranged in ductal or sheet-like structures. (H&E. **a** ×10. **b** ×50)

**Table 1** Characteristics of pleomorphic adenoma arising from the periphery of the lung

| Case | Author | Age (years) | Gender | Symptoms | Size (cm) | Metastasis | Treatment | Follow-up |
|---|---|---|---|---|---|---|---|---|
| 1 | Wright [7] | 74 | F | Lethargy, Dyspnea | 4.5 | None | Surgical resection | No recurrence |
| 2 | Sakamoto et al. [5] | 56 | F | None | 2.5 | None | Surgical resection | Contralateral lung metastasis 9 years later |
| 3 | Moran et al. [4] | 45 | F | None | 2.5 | None | Surgical resection | Died 4 years later from breast cancer recurrence |
| 4 | Moran et al. [4] | 57 | M | None | 2 | None | Surgical resection | Died in postoperative period from myocardial infarction |
| 5 | Moran et al. [4] | 69 | F | None | 2 | None | Surgical resection | Lost to follow-up |
| 6 | Takeuchi [6] | 48 | F | Lumbago | 4.3 | Bone, lymph node, liver, lung | Palliative RT for bone metastasis | Alive 19 months later |
| 7 | Hara [8] | 38 | F | None | 4 | None | Surgical resection | No recurrence |
| 8 | Carretta [9] | 22 | F | None | 2.4 | None | Surgical resection | No recurrence 2 years later |
| 9 | Jin [10] | 25 | F | None | 2.8 | None | Surgical resection | Unknown |
| 10 | Present | 76 | M | None | 1.3 | None | Surgical resection | Pleural dissemination 2 years later |

*RT* radiation therapy

In the present case, histopathological findings showed scant mitosis, necrosis, and cellular atypia, though visceral pleural surface invasion was suspected as low grade malignancy. Among the other cases, local recurrence was seen in 3 patients, of whom 2 had recurrence in the surgical margin. Therefore, it is necessary to pay attention to tumor implantation and the surgical margin. We performed a wedge resection with a sufficient surgical margin in spite of visceral pleural surface invasion and adhesion to the parietal pleura. However, even though a complete resection was done, a relapse occurred. To the best of our knowledge, the present is the first case that developed as pleural dissemination.

A CTGNB was performed preoperatively for diagnosis in the present case. This is a useful procedure for diagnosing pulmonary lesions, particularly in cases with small-sized nodules in peripheral lung tissue [13]. However, the procedure may cause tumor dissemination in cases of malignancy. Sawabata and colleagues [14] suggested that a fine-needle aspiration biopsy procedure has a potential to spread malignant cells to the pleural space, though it remains unknown how disseminated malignant cells mature into tumor masses. Recently, Inoue et al. [15] reported that CTGNB was associated with a higher risk of local recurrence as pleural dissemination in stage I lung cancer patients. In addition, they showed that subpleural lesions had a higher risk of pleural relapse. Thus, in the present case, CTGNB might have been associated with development of pleural dissemination.

In summary, a pleomorphic adenoma arising in the peripheral lung is a rare phenomenon. In the present case, we noted a rare recurrence pattern of pleural dissemination

**Table 2** Characteristics of patients with recurrence or metastasis after initial operation

| Case | Author | Age (years) | Gender | Location | Size (cm) | Gross features | Recurrence |
|---|---|---|---|---|---|---|---|
| 1 | Payne et al. [2] | 50 | F | Right bronchus intermedius | 2 | Poorly defined mass | Recurrence 8 years later at bronchial stump and right hilar region |
| 2 | Spencer [3] | 68 | M | Right lower lobe | Unknown | Large mass, occupying much of a lobe | Metastasis to lumbar vertebra 4 years later |
| 3 | Sakamoto [5] | 56 | F | Right upper lobe | 2.5 | Round with a smooth surface and clearly demarcated mass | Recurrence 9 years later in the contralateral lung |
| 4 | Moran [4] | 35 | F | Right lower lobe | 16 | Poorly circumscribed mass, replacing nearly entire lobe | Recurrence 2 years later in right medial and posterior hemithorax |
| 5 | Moran [4] | 67 | M | Right upper lobe | 6 | Poorly circumscribed mass | Recurrence 3 years later in trachea and right mainstem bronchus |
| 6 | Present | 76 | M | Right middle lobe | 1.3 | Well-circumscribed mass | Pleural dissemination 2 years later |

with this neoplasm. Although it is not clear whether CTGNB was related to pleural dissemination in our patient, we recommend that clinicians avoid performing a percutaneous needle biopsy for subpleural lesions with suspected malignancy because there may be a potential to spread malignant cells through the tract. In addition, careful follow-up examinations are mandatory because of possible aggressive behavior.

## Conclusion

We performed surgery for a patient with a pleomorphic adenoma arising from peripheral lung tissue, which later showed recurrence as pleural dissemination. It should be kept in mind that recurrence may develop with this neoplasm because of malignant potential.

## References


1. Moran CA. Primary salivary gland-type tumors of the lung. Semin Diagn Pathol. 1995;12:106–22.
2. Payne WS, Schier J, Woolner LB. Mixed tumors of the bronchus (salivary gland type). J Thorac Cardiovasc Surg. 1965;49:663–8.
3. Spencer H. Bronchial mucous gland tumours. Virchows Arch A Pathol Histol. 1979;27:101–15.
4. Moran CA, Suster S, Askin FB, Koss KN. Benign and malignant salivary gland-type mixed tumors of the lung. Clinicopathologic and immunohistochemical study of eight cases. Cancer. 1994;73:2481–90.
5. Sakamoto H, Uda H, Tanaka T, Oda T, Morino H, Kikui M. Pleomorphic adenoma in the periphery of the lung. Report of a case and review of the literature. Arch Pathol Lab Med. 1991;115:393–6.
6. Takeuchi E, Shimizu E, Sano N, Yamaguchi T, Yanagawa H, Sone S. A case of pleomorphic adenoma of the lung with multiple distant metastases—observations on its oncogene and tumor suppressor gene expression. Anticancer Res. 1998;18:2015–20.
7. Wright ES, Pike E, Couves CM. Unusual tumours of the lung. J Surg Oncol. 1983;24:23–9.
8. Hara M, Sato Y, Kitase M, Nakayama J, Ohba S, Kaji M, Yamakawa Y, Tateyama H. CT and MRI findings of a pleomorphic adenoma in the peripheral lung. Radiat Med. 2001;19:111–4.
9. Carretta A, Libretti L, Taccagni G, Zannini P. Salivary gland-type mixed tumor (pleomorphic adenoma) of the lung. Interact Cardiovasc Thorac Surg. 2004;3:663–5.
10. Jin HY, Park TS. Pulmonary pleomorphic adenoma: report of a rare case. Korean J Intern Med. 2007;22:122–4.
11. Friedrich RE, Li L, Knop J, Giese M, Schmelzle R. Pleomorphic adenoma of the salivary glands analysis of 94 patients. Anticancer Res. 2005;25:1703–5.
12. Rodríguez-Fernández J, Mateos-Micas M, Martínez-Tello FJ, Berjón J, Montalvo JJ, Forteza-González G, Galan-Hernández R. Metastatic benign pleomorphic adenoma. Report of a case and review of the literature. Med Oral Patol Oral Cir Bucal. 2008;13:E193–6.
13. Tomiyama N, Mihara N, Maeda M, Johkoh T, Kozuka T, Honda O, Hamada S, Yoshida S, Nakamura H. CT-guided needle biopsy of small pulmonary nodules: value of respiratory gating. Radiology. 2000;217:907–10.
14. Sawabata N, Ohta M, Maeda H. Fine-needle aspiration cytologic technique for lung cancer has a high potential of malignant cell spread through the tract. Chest. 2000;118:936–9.
15. Inoue M, Honda O, Tomiyama N, Minami M, Sawabata N, Kadota Y, Shintani Y, Ohno Y, Okumura M. Risk of pleural recurrence after computed tomographic-guided percutaneous needle biopsy in stage I lung cancer patients. Ann Thorac Surg. 2011;91:1066–71.

# Thin-section CT findings in peripheral lung cancer of 3 cm or smaller: are there any characteristic features for predicting tumor histology or do they depend only on tumor size?

Binghu Jiang, Shodayu Takashima, Chie Miyake, Tomoaki Hakucho, Yoshiyuki Takahashi, Daisuke Morimoto, Hodaka Numasaki, Katsuyuki Nakanishi, Yasuhiko Tomita and Masahiko Higashiyama

*Acta Radiol* published online 7 August 2013
DOI: 10.1177/0284185113495834

Acta Radiol OnlineFirst, published on August 7, 2013 as doi:10.1177/0284185113495834

*Original Article*

Acta Radiologica
0(0) 1–7

DOI: 10.1177/0284185113495834
acr.sagepub.com

# Thin-section CT findings in peripheral lung cancer of 3 cm or smaller: are there any characteristic features for predicting tumor histology or do they depend only on tumor size?

**Binghu Jiang[1,2], Shodayu Takashima[1], Chie Miyake[1], Tomoaki Hakucho[1], Yoshiyuki Takahashi[1], Daisuke Morimoto[1], Hodaka Numasaki[1], Katsuyuki Nakanishi[3], Yasuhiko Tomita[3] and Masahiko Higashiyama[3]**

## Abstract

**Background:** Ground-glass opacity (GGO) is reported to be characteristic to lepidic growth of neoplasm in subsolid nodules. In solid nodules of lung cancer, however, there is no characteristic feature to be reported.

**Purpose:** To study if there are any thin-section CT findings characteristic to tumor histology or if they are only related to tumor size in solid nodules of the lung cancer.

**Material and Methods:** This study included 106 solid peripheral lung cancers of 3 cm or smaller (56 adenocarcinomas, 33 squamous cell carcinomas, and 17 small cell carcinomas) in which 16-slice CT with 1 mm collimation was performed before surgery. Six morphologic findings (presence or absence of lobulation, coarse spiculation, air bronchogram, cavity, pleural tag, and pleural-based lesion) and four measurements (ratio of the greatest transverse and vertical diameter to the shortest transverse diameter and density of lobulation and coarse spiculation) on thin-section CT images were evaluated. Density of lobulation (coarse spiculation) was defined as the ratio of lobulation (coarse spiculation) number to the greatest transverse diameter of a nodule.

**Results:** Air bronchogram ($P < 0.01$) was the only significant factor for predicting lung adenocarcinoma. The prevalence of air bronchogram was significantly greater in adenocarcinoma than in squamous cell carcinoma ($P < 0.01$) or small cell carcinoma ($P < 0.01$). As the tumor size advanced, significantly positive linear trends were seen in the prevalence of lobulation ($P < 0.01$), coarse spiculation ($P < 0.01$), and pleural tag ($P < 0.01$), and the mean values of density of lobulation ($P < 0.01$) and coarse spiculation ($P < 0.01$), while the significant negative linear trend was seen in the ratio of vertical diameter to the shortest transverse ($P = 0.02$).

**Conclusion:** Air bronchogram on thin-section CT is characteristic feature of solid adenocarcinoma of the lung. However, other thin-section CT findings are irrelevant to tumor histology and related only to tumor size.

**Keywords**
Lung neoplasms, air bronchogram, computed tomography, CT findings

Date received: 15 March 2013; accepted: 1 June 2013

## Introduction

According to recent global cancer statistics, lung cancer is the most common form of cancer and the leading cause of cancer death (1). As for the histology of lung cancer, adenocarcinoma, which accounts for 38.5% of

[1]Department of Diagnostic Radiological Imaging, Division of Allied Health Sciences, Osaka University Graduate School of Medicine, Osaka, Japan
[2]Thoracic Medical Center, BenQ Hospital, Nanjing Medical University, Nanjing, China
[3]Osaka Medical Center for Cancer and Cardiovascular Diseases, Osaka, Japan

**Corresponding author:**
Binghu Jiang, Department of Diagnostic Radiological Imaging, Division of Allied Health Sciences, Osaka University Graduate School of Medicine, 1–7 Yamadaoka, Suita City, 565-0871, Japan.
Email: mbhh@live.cn